Rate dependent image distortions in proportional counters

M. W. Trow[1], A. C. Bento[2], A. Smith[1]

1. Department of Space and Climate Physics, University College London,
Mullard Space Science Laboratory, Holmbury S[t] Mary, Dorking, Surrey,
RH5 6NT UNITED KINGDOM

2. Department of Physics, University of Coimbra,
P-3000 Coimbra PORTUGAL

Published in Nuclear Instruments and Methods in Physics Reasearch A 348 (1994) 232-236
(Proceedings of the Third London Conference on Position Sensitive Detectors, Brunel, September 1993)

The positional linearity of imaging proportional counters is affected by the intensity distribution of the incident radiation. A mechanism for this effect is described, in which drifting positive ions in the gas produce a distorting electric field which perturbs the trajectories of the primary electrons. In certain cases, the phenomenon causes an apparent improvement of the position resolution.

We demonstrate the effect in a detector filled with a Xenon-Argon-CO_2 mixture. The images obtained are compared with the results of a simulation. If quantitative predictions for a particular detector are required, accurate values of the absolute detector gain, ion mobility and electron drift velocity are needed.

Rate Dependent Effects In Proportional Counters

Position sensitive proportional counters are used in a variety of applications for detection of XUV and X-ray photons and other radiation. The dynamic range of these detectors has previously been limited by the position readout electronics, but several recent readout designs are capable of functioning at the maximum rate of the counter.

Hell et. al [1] observed image distortions at rates of 15 to 30 MHz/cm^2 of Mo-k radiation, in an MWPC having a 9 mm drift gap. The gas used was Ar + 1% CO_2 at 4 and 8 bar. Dmitriev and Frumkin [2] have described their experiences of these effects. They used a similar chamber with a drift gap of 10 mm, and found measurable distortions at rates of a few tens of kHz. Their detector was filled with Ar + 18% CO_2 at a pressure of 1 atm.

The distortions had the following characteristics, not all of which were observed simultaneously: distortion of beam profiles, decrease of apparent beam width, apparent improvement of the position resolution, separate profiles moving closer together, and smearing of profiles near intense illumination.

These distortions occurred in conjunction with a count-rate dependent change of the gas gain. In a readout system whose lower level discriminator is set near the low energy tail of the usual pulse height distribution, this is accompanied by a loss in counting efficiency. Both effects are due to the electric field contribution of the positive ions produced in the avalanches. The general principles of ion induced gain depression were outlined by Hendricks [3] and further treatments can be found in references [4 to 8].

Distortion Mechanism

Immediately following an electron avalanche in a proportional counter, that is, after all the electrons have reached the anode wire, a cloud of positively ionised gas atoms or molecules begins to drift toward the cathode [9]. The resulting distribution of ions can be calculated if the electric field in the detector is known.

In the special case of a coaxial detector in which avalanches are distributed uniformly around the anode wires, a constant counting rate produces a uniform density of ions. The charge density ρ for a count rate n is given by:

$$\rho = \frac{nq\,\varepsilon_0}{\mu VC},$$

where q is the avalanche charge, V is the anode voltage and C is the capacitance per wire per unit length. μ is the ion mobility, and ε_0 is the permittivity of free space. This expression can also be applied near the anodes of other types of detector.

When a detector is illuminated by a narrow beam or point, a sheet of ions will be produced in the drift regions. This charge generates an electric field which has a component perpendicular to the plane of the sheet. Primary electrons are attracted to this region of ion density as they drift toward the anode. See Fig 1.

The amount of lateral drift will depend on the density of ions in the sheet, the location of the primary ionisation, and the drift velocity of the electrons. At any point in the electron's path, the direction of drift is that of the gradient of the total electric field, and the drift velocity is a complex function of the field strength. This function is usually highly dependent on the proportions of the gas mixture.

The magnitude of perturbing field of the ion sheet decreases with distance. Therefore, photons absorbed close to the ion sheet will drift more than those absorbed further away. In addition, the perturbing field is weaker near the edges of the ion distribution, i.e. near the cathodes or between the wires in a MWPC, than in the centre of the drift volume. An electron whose trajectory which begins at the upper cathode will drift more than an electron absorbed close to the anode wire, because the latter experiences sideways drift for a shorter time. Since the sites of initial ionisation occur at range of depths in the gas, it can be expected that a distribution of lateral drifts will be observed for a particular initial perpendicular distance from the ion sheet.

Practical consequences

Each point in an image will produce its own positive ion sheet, which can affect the electron trajectories in all other parts of the detector. The trajectories of the ions will also be modified by the distribution of ions, although the magnitude of this effect will be smaller due to the ion's lower mobilities. The result will be that bright regions in any image will attract one another, and the degree of attraction will be a function of the count rate. Certain regions in the recorded image will increase in intensity, and others parts may decrease. The overall number of counts in the image is unchanged, unless a greater number of pulses fall below the readout system's lower level discriminator due to gain-related changes in the pulse height distribution.

In a flat field, or rectangular image, the centre of attraction will be the centre of the field. There will be an enhancement of intensity near the centre of the image, and a decrease at the edges.

Distortions in images of a number of small, bright points, separated by regions of low intensity, will appear largely as motion of the points towards their common centre. However, since the shifts depend on the depth of photon absorption, the profiles of the points will become skewed. If the size of the features is less than the position resolution of the system, the skew of the distorted profiles can result in a worsening of the measured resolution.

Medium sized features, with scale lengths a few times larger than the position bin width, can affected in the opposite way. If there are no features nearby that can significantly affect the centroid of the feature, and the intensity of the feature is sufficient to cause distortions, the profile will remain symmetrical but decrease in width (self-focusing). The measured position resolution will therefore appear to improve.

In many systems, the position resolution is limited by the gas, and the point spread function is over-sampled by the readout electronics. Position resolution measurements are very often made with test images consisting of small points separated by large regions of zero intensity. Under these conditions, one can obtain an anomalous improvement of the resolution with higher count rate, without any measurable change of the centroid of the points.

Tests with a position sensitive proportional counter

To determine the effect of counting rate on a test image, we illuminated a position sensitive detector through a mask mounted against its window. Table 1 describes the detector used for these tests. Identical detectors were flown in the *Yohkoh* Bragg Crystal Spectrometer [10], which is used to

study the soft X-ray emission of solar flares, and their performance has been described elsewhere [11, 12].

The mask was a 0.9 mm thick sheet of Aluminium with a slit and pinholes. The slit was perpendicular to the axis of the anode wires, and the holes were arranged along a line parallel to the anodes at various distances from the slit: 5, 4, 3, 2, and 1 mm on one side and 1.5, 2.5, 3.5, 4.5 and 5.5 mm on the other. Each hole had an area of 0.79 mm^2 (diameter 0.5 mm), and the slit, of width 0.5 mm, had an area of 6 mm^2 (accounting for the effect of the window support structure). The length of the slit was such that only one anode was illuminated. The slit was positioned halfway along the length of the detector, and the holes were positioned 3 mm perpendicularly from the active anode.

An Nb target X-ray source with an aperture of 3 mm diameter was positioned 127 cm from the centre of the detector. Radiation entered the detector normally through the slit, but at an angle of 0.22 ° to the normal through the furthest hole. However the mean depth for absorption for Nb-L X-rays in this particular gas is approximately 2 mm, so this parallax did not affect the measured position of the hole profiles.

Charge sensitive preamplifiers (Amptek A250) connected to anodes and readout cathodes were used to obtain signals for each event, and the pulses were routed to commercial shaping amplifiers. The height of each pulse was determined by 12 bit ADCs and the data acquired by a computer, which calculated the position of each event by dividing the induced charge signal from one of the cathode's “wedges” by the sum of the charge on both wedges [11].

We obtained a number of images of the mask at anode voltages of 1480, 1510, 1540 V and count rates from 100 Hz to 2 kHz. The central slit was obscured at the lowest gain.

A typical sequence of images is shown in Fig 2.

These plots show the profiles of the pinholes moving towards the central region, and becoming merged together. A “tail” can be seen on the side of the outer profiles. The inner pinholes are affected first, but the whole image is affected at the higher rates. The contrast in the image is poor at higher rates.

Each image was analysed in turn by a peak finding and fitting program. This was able to fit a Gaussian to each pinhole image if it was distinct from its neighbour.

The total width of the image (the difference between the centroids of the two peaks at either edge of the group) was determined, and is plotted against count rate in Fig 3. The data consists of images taken at 1480 V with the slit closed and with the slit open. The width at the lowest rate (300 Hz) was taken to be 1.0, and the other widths are relative to this.

The contrast, defined here as the ratio of the maximum of a peak to the average of the minima on either side, was returned by the fitting procedure. This definition is not meaningful for the extreme peaks, at its value depends on the spacing of the features and the intrinsic position resolution. Fig 4 shows the contrast as a function of count rate for the first non-extreme peak in the image, which relates to a pinhole 4.5 mm from the slit centre. Again, the data is for 1480 V with slit open and with slit closed.

Results of a Simulation.

A numerical model of the image distortion effect was developed by the authors. The two-dimensional form of the anode field was first determined using a finite element method. This was then used to compute the distribution of a sheet of ions at unit count rate, using a particle following algorithm.

We assumed that all avalanches were uniformly distributed in azimuth angle around the wire. A large number (~1000) of equal angle increments were selected, and for each angle, the trajectory of the ion in the anode field was determined. The volume of the detector was divided into rectangular elements, and the ion density computed by accumulating for each element the number of tracks which passed through the element, weighted by the time taken to cross the element. For simplicity, we assumed that the ions did not interact with one another, and that diffusion was negligible. The resulting density array was stored for later use. For an arbitrary count rate, the densities were scaled appropriately.

Electron trajectories were calculated by computing the field contribution of a single thin ion sheet at various points in the detector, and following the history of a test electron. We assumed that the test particle did not produce any ions, so that the only interaction was between a single electron and the sheet of ions. In addition, we approximated the electron drift velocity function with a simple linear relationship, that is, we defined a constant electron mobility.

At any point in the detector, the electric field of the ion sheet was found by summing the contributions from each of the rectangular elements in the ion density grid. Combining this with the anode field gave the total field, and hence the electron drift velocity. The test electron was then moved an appropriate distance, and the field calculation repeated at its new location, until the electron reached the anode.

The calculations were repeated for positions similar to those used in the test mask, and for a range of count rates. The results are summarised in Fig. 5.

Discussion

The modelled results are well approximated by a family of exponential functions describing the position shift as a function of distance from the central bright region:

$$\text{shift} = A\,\mathbf{exp}(-x / d),$$

where A is a parameter depending on the count rate, x is the distance of the test peak from the bright region and d is a scale length parameter. We find that d = 8.3 mm best describes the model results.

It is clear that the modelled shifts are not large enough to account for the distortions seen in practice. In addition, the exponential law followed by the model was not confirmed in the experiment. The former suggests that some physical parameters used in the model are incorrect, and the latter that the model was not sufficiently representative of the experimental situation.

The physical parameters that seem most likely to affect the size of the shifts are those which affect the total number of ions in the drift region, namely the ion mobility and the gain. In the absence of any values in the literature, we took the ion mobility to be that of Xenon in its own gas. The gain was estimated as 1.5×10^4 at 1480 V, which may be somewhat lower than the true value due to ballistic deficit in the shaping amplifiers.

In compiling the model results, we assumed that the smaller images would not influence one another compared with the bright slit, and so we calculated the position shift for each separately. The assumption was shown to be invalid by the data obtained with the slit closed, where the pinhole images were seen to bunch together such that the inner pair (closest to the slit position) moved away from one another.

Conclusion

We have demonstrated rate dependent image distortions in a one-dimensional position sensitive proportional counter. Whilst this counter was not intended for use in high rate applications, it did allow us to study the effect at moderate rates and with conventional equipment. In particular, the "slow" gas mixture and large drift volumes, combined with the relatively deep drift region, contributed to the magnitude of this phenomenon.

If one wishes to avoid this type of behaviour, the gas mixture and geometry must be chosen accordingly, so as to minimise the density of ions in the detector volume.

Predictive models of the effect require as a starting point a good description of the electric field everywhere in the detector, and appropriate values for the electron drift velocity and ion mobility. If complex images are to be studied at high rate and high positional accuracy, the models should be configured with those types of images in mind.

Acknowledgements

The authors would like to thank colleagues at their institutes for their support and encouragement, and for many stimulating discussions.

References

1 E. Hell, H. J- Besch, L. Brabetz, P. Kuhn and A. H. Walenta, *Position resolution, high rate behaviour and space charge induced image distortion of a multiwire X-ray detector for digital subtraction angiography*, Nucl. Instr. and Meth., A269 (1988) 404.

2 G. D. Dmitriev and I. B. Frumkin, *A study of MWPC accuracy of X-ray coordinate sensing at high counting rate*, Nucl. Instr. and Meth., A295 (1990) 384.

3 R.W. Hendricks, *Space charge effects in proportional counters*, Rev. Sci. Instrum, 40-9 (1969) 1216-1223.

4 H. Sipila, V. Vanha-Honko, *The counting rate dependent gain shift and the space charge in proportional counters*, Nucl. Instr. and Meth., 153 (1978) 461.

5 H. Sipila, V. Vanha-Honko, J. Bergqvist, *Mathematical treatment of space charge effects in proportional counters*, Nucl. Instr. and Meth., 176 (1980) 381.

6 E. Mathieson, *Dependence of gain on count rate, due to space charge, in coaxial and multiwire proportional chambers*, Nucl. Instr. and Meth., 249 (1986) 420.

7 G. C. Smith, E. Mathieson, *Gain reduction due to space charge at high counting rates in multiwire proportional chambers*, IEEE Trans. Nucl. Sci, NS-34 (1987) 410.

8 E. Mathieson and G. C. Smith, *Gain reduction due to space charge in a multiwire proportional chamber irradiated by a uniform beam of rectangular section*, Nucl. Instr. and Meth., A316 (1992) 246.

9 F. Sauli, *Principles of operation of multiwire proportional and drift chambers*, CERN Report 77-09 (1977).

10 J. L. Culhane, E Hiei, G. A. Doschek, A. M. Cruise, Y. Ogawara, Y. Uchida, R. D. Bentley, C. M. Brown, J. Lang, T. Watanabe, J. A. Bowles, R. D. Deslattes, U. Feldman, A. Fludra, P. Guttridge, A. Henins, J. Lapington, J. Magraw, J. T. Mariska, J. Payne, K. J. H. Phillips, P. Sheather, K. Slater, K. Tanaka, E. Towndrow, M. W. Trow and A Yamaguchi, *The Bragg crystal spectrometer for Solar-A*, Solar Physics 136 (1991) 89.

11 M. W. Trow, J. S. Lapington, R. D. Bentley, *Position sensitive detector with wedge-and-wedge readout*, Nucl. Instr. and Meth., A310 (1991) 344.

12 M. W. Trow, *Performance of the position sensitive proportional counters of the Yohkoh Bragg crystal spectrometer*, ESA SP-356 (1992) 383.

13 R. Allemand and G. Thomas, *Nouveau Detecteur de localisation*, Nucl. Instr. and Meth., 131 (1976) 141.

14 B. P. Duval, J. Barth. R. D. Deslattes, A. Henins and G. G. Luther, *Position-sensitive X-ray detector*, Nucl. Instr. and Meth., 222 (1984) 274.

Figures & Tables

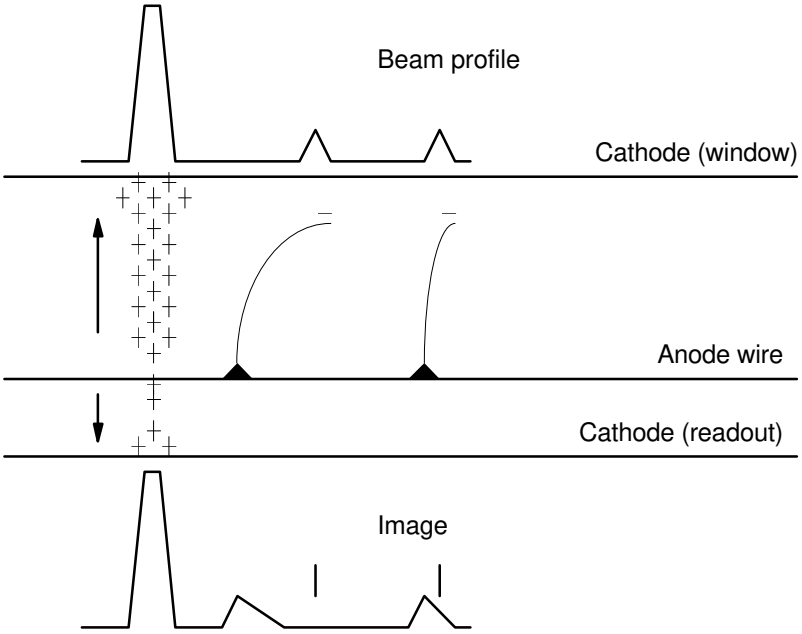

Fig 1. Longitudinal cross section of a proportional counter showing an anode wire and two cathode planes. Radiation with the intensity distribution shown enters through the upper cathode, and the resulting avalanches produce an ion distribution mainly in the regions marked with (+). Electron trajectories (-) of photons absorbed nearby are attracted to the ion-filled region, and the recorded image is distorted.

Internal Cross section (D×W)	20 mm × 48 mm × 2 sections
Active area (L×W)	89 mm × 44 mm × 2 sections
Body material	stainless steel
Window	125 μm Be
Readout	Backgammon [13, 14] type (1-D charge division)
Gas fill (permanently sealed)	47.5% Xe, 47.5% Ar, 5% CO_2
Pressure	1.2 atm
Typical anode voltage	1480 V
Anode (diameter, material)	15 μm, Pt-W
Number of anodes (per section)	2
Anode spacing	16 mm
Anode distance to cathode (readout)	3.2 mm
Anode distance to cathode (window)	16.8 mm

Table 1. Properties of the position sensitive proportional counter.

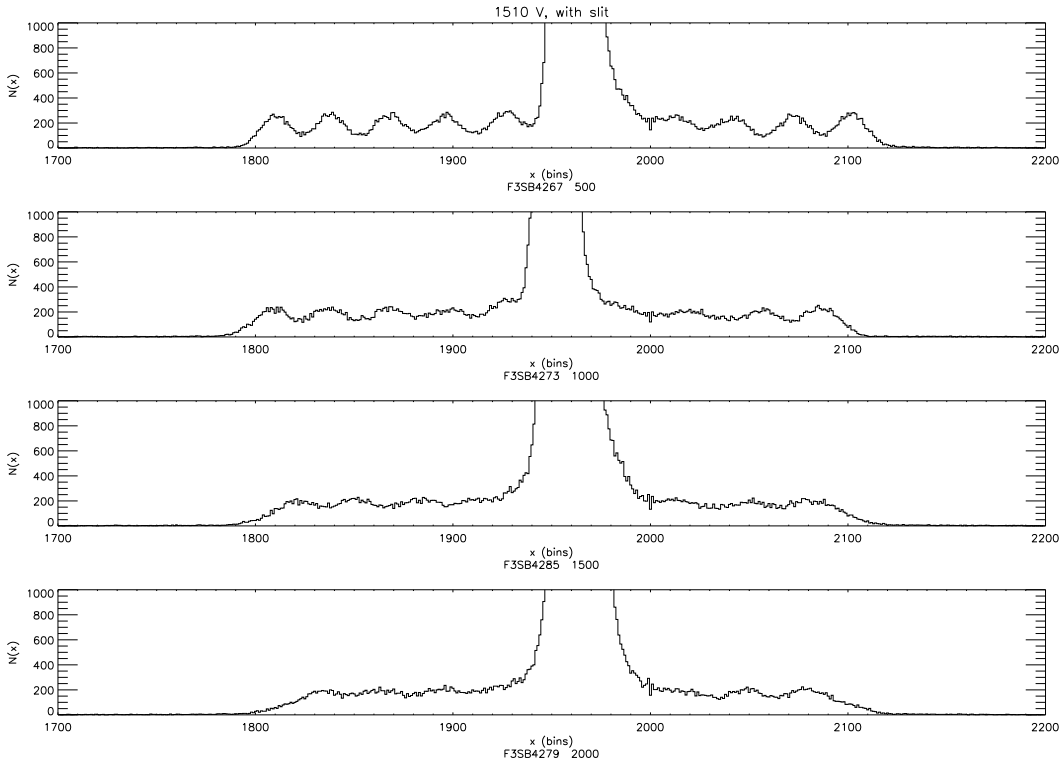

Fig 2. Images of a slit and pinholes at increasing rates, showing distortion of the image and loss of contrast. 2.2 keV X-rays, anode at 1510 V. Rates (per second) of 500 (top), 1000, 1500 and 2000 (bottom).

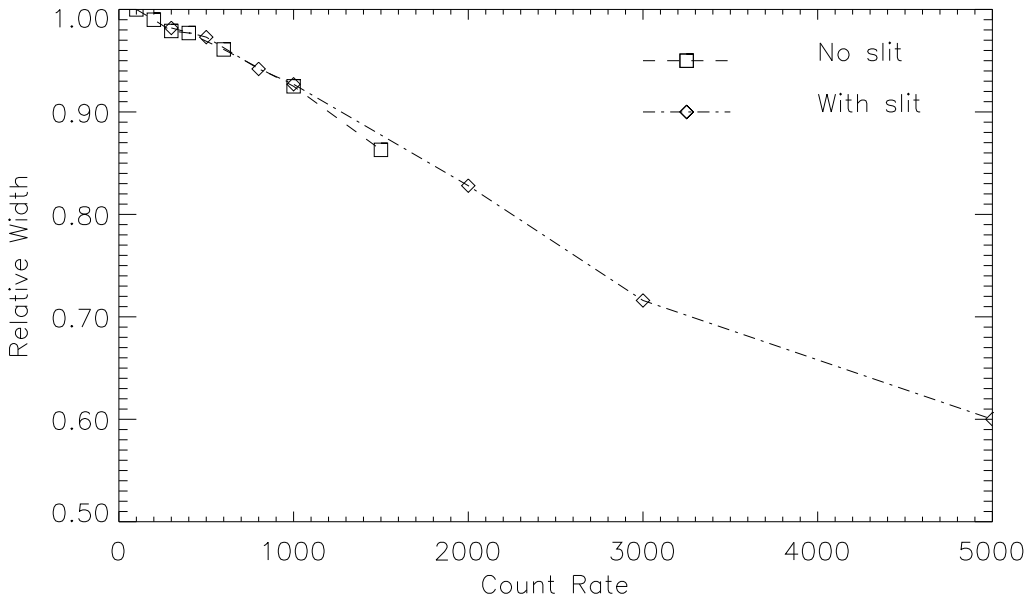

Fig 3. Total width (difference of centroids of the features at the edge of the test pattern) vs. count rate. Two data sets were analysed, both with anode at 1480 V, with central bright slit and without. All data were scaled so that the width of the lowest rate image is 1.0. The actual separation of the features was 10.5 mm

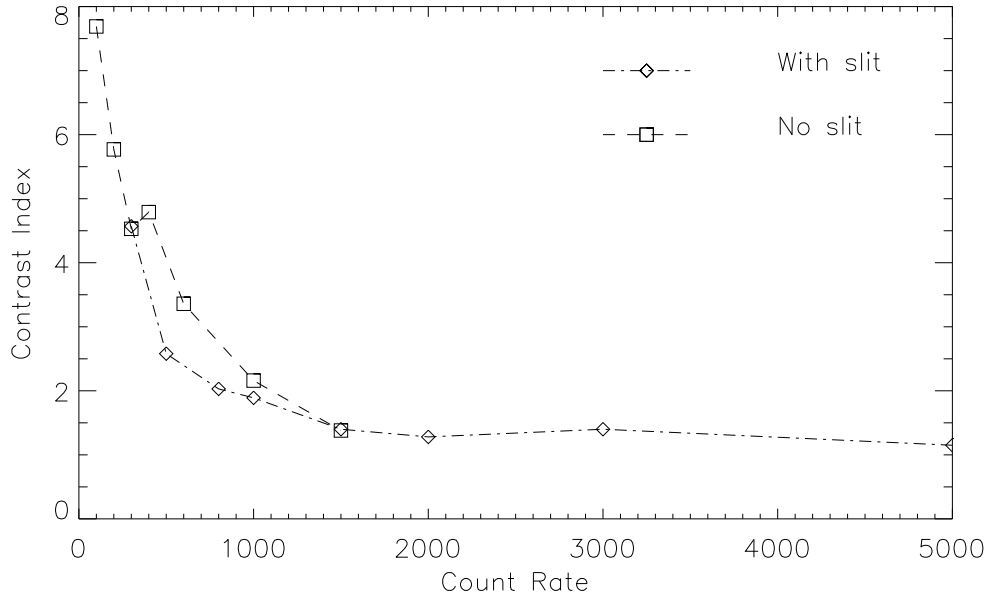

Fig 4. Contrast index vs. count rate, anode at 1480 V. This is the contrast (defined in text) of a feature 4.5 mm from the centre of the test pattern.

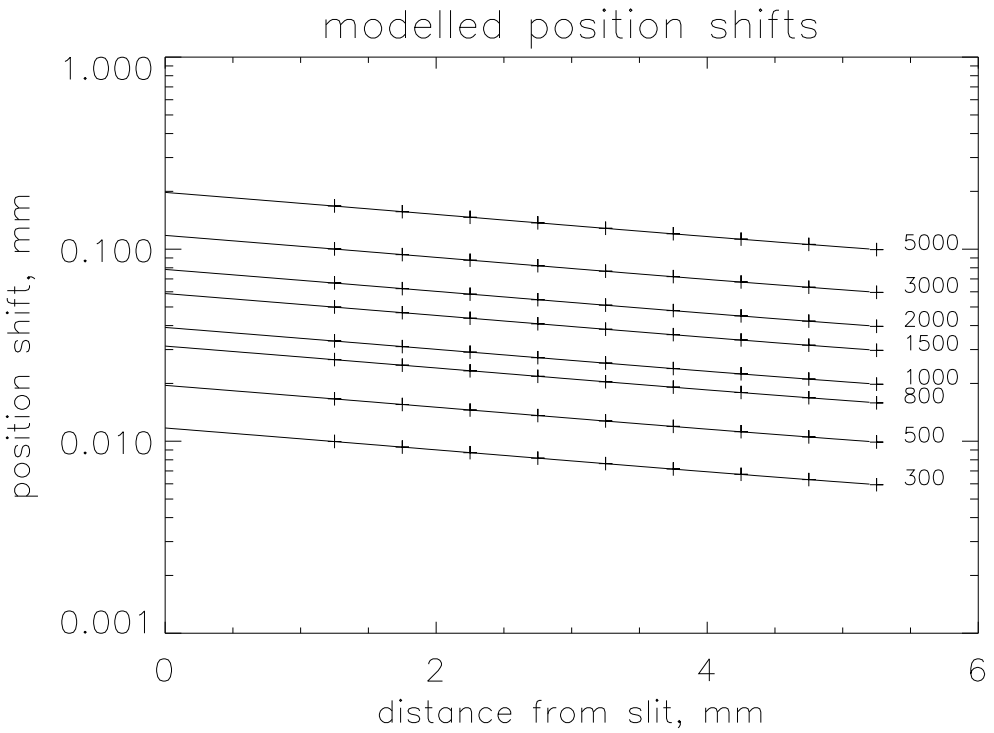

Fig 5. Summary of model results, showing the position shift vs. actual position for a series of count rates, as marked.